J. Cent. South Univ. (2017) 24: 546−559
DOI: 10.1007/s11771-017-3457-1

Springer

Effect of fin attachment on thermal stress reduction of exhaust manifold of an off road diesel engine

Ali Akbar Partoaa, Morteza Abdolzadeh, Masoud Rezaeizadeh

Department of Mechanical Engineering, Graduate University of Advanced Technology, Kerman, Iran

Abstract: The effect of fin attachment on the thermal stress reduction of exhaust manifold of an off road diesel engine (Komatsu HD325-6) was investigated. For doing this, coupled thermo-fluid-solid analysis of exhaust manifold of the off road diesel engine was carried out. The thermal analysis, including thermal flow, thermal stress, and the thermal deformation of the manifold was investigated. The flow inside the manifold was simulated and then its properties including velocity, pressure, and temperature were obtained. The flow properties were transferred to the solid model and then the thermal stresses and the thermal deformations of the manifold under different operating conditions were calculated. Finally, based on the predicted thermal stresses and thermal deformations of the manifold body shell, two fin types as well as body shell thickness increase were applied in the critical induced thermal stress area of the manifold to reduce the thermal stress and thermal deformation. The results of the above modifications show that the combined modifications, i.e. the thickness increase and the fin attachment, decrease the thermal stresses by up to 28% and the contribution of the fin attachment in this reduction is much higher compared to the shell thickness increase.

Key words: manifold; exhaust; simulation; modification; thermal stress; deformation; diesel engine

1 Introduction

Exhaust manifold delivers the hot outlet gases of combustion products through the tail pipe to the atmosphere. The manifold body should have an appropriate thermal resistance against thermal stresses up to 1000 °C. The manifold's metal is fatigued when it repeatedly becomes hot and cold and thus special attention should be placed on the criteria like the induced maximum temperature and thermal expansion due to the combustion heat transfer. Thermal stress is a complex and important phenomenon in the solid mechanics analysis of the manifold. Determination of the temperature distribution of the manifold solid body is essential to evaluate the effects of thermal stress on the manifold failure. In some engineering applications, thermal stresses are more destructive than the mechanical stresses and therefore more focuses should be designated on the evaluation of the manifold thermal stresses. So far, many studies have investigated the effects of thermal stress on the exhaust manifold.

KANDYLAS et al [1] developed a model and investigated its performance in two exhaust piping arrangements, i.e., single wall and double wall with air gap or insulation. LONDHE [2] studied the effect of thermal stresses on the exhaust manifold, cylinder head, and turbocharger. YASAR et al [3] studied an exhaust manifold equipped with a cooling system. They investigated the thermo-mechanical stresses under different flow rates of coolant fluid flow. They showed that some modification can decrease the thermal stresses up to 30%. ZHANG [4] studied the welding residual stresses in an exhaust manifold. He showed that consideration of these stresses gives a higher accuracy for prediction of the analysis of thermal stresses. MAOQINA [5] carried out the thermo-solid-fluid analysis of a stainless steel exhaust manifold. They evaluated thermal resistant strength and safety factor of the exhaust manifold and then based on them the reliability of the design was determined.

RATHNARAJ [6] revealed that at high intensive operating conditions of an engine, a very high thermal stress is found and it causes to create a deep crack in the manifold. He also examined the working life of the manifold under different thermal stress conditions.

SATISH [7] carried computational thermal simulation of a gasoline engine. They also performed an experimental measurement and compared them with the simulation results. They found a good agreement between the experimental results and the numerical results.

Received date: 2015−11−12; **Accepted date:** 2016−02−08
Corresponding author: Morteza Abdolzadeh, PhD; Tel: +98−3433776612; E-mail: m.abdolzadeh@kgut.ac.ir

LIU [8] predicted the thermal stresses of an exhaust manifold in transient and steady state conditions. They revealed a high temperature difference between the transient and steady state conditions and recommended study of the transient analysis of the exhaust manifold. JAIN et al [9] simulated an exhaust manifold and obtained the thermal stresses and the manifold deformations. They investigated thermo-mechanical stresses of two cast iron and steel manifolds. They showed that the cast iron manifold resists better against the thermal stresses at higher operating temperatures of the manifold compared to the steel one. ZOU [10] investigated the effect of outlet gas temperature in two exhaust manifolds with different materials, namely ductile and Si-Mo ductile cast irons. They revealed that molybdenum in the cast iron has an effective role in the reduction of thermal stresses and increases the operating life of the manifold.

LUJAN et al [11] evaluated the some correlations proposed by other studies for four stroke engines and presented a new heat transfer model for exhaust systems in two-stroke, high performance, gasoline engines. Comparisons of their proposed model with other models showed negligible differences in the scavenge process related parameters.

Based on the reviewed literature, different characteristics of exhaust manifolds such as geometry, shape, solid and gaseous materials, and areas of inlet and outlet sections affect the manifold thermal stress. Modifications like increasing the thickness of the manifold solid body and improvement of heat transfer significantly decreases the manifold thermal stresses. This work aims to evaluate the effects of fin attachment on the heat transfer improvement of a manifold to reduce the crack creation due to thermal stresses in the manifold body. For doing this, the effect of fin attachment on thermal stress reduction of a cracked exhaust manifold of an off road diesel engine (Komatsu HD325-6) was investigated. First, the cracked exhaust manifold of the diesel engine was computationally simulated and the exhausted gas flow and the manifold body were analyzed. Second, thermal stresses and thermal deformations were obtained all over the manifold body and the critical regions as well as the place of manifold cracks were predicted. Then, some fins were attached to the body where the high thermal stresses occurred and the modified body was simulated. Finally, the reduction of the thermal stresses was investigated.

2 System description and simulation process

As mentioned earlier, the exhaust manifold of Komatso HD-325 off road diesel engine was simulated (Fig. 1). This manifold has six gas inlets and two outlets. The products of combustion enter into the exhaust manifold with 750 °C temperature at the maximum engine speed (Based on the engine specifications) and then cross the engine turbocharger. This maximum temperature and also the variation of the combustion product temperature at different engine speeds have created a deep crack in the outlet section of the manifold, (Fig. 1). This crack has caused the engine to not operate efficiently. The modeled manifold is shown in Fig. 2. This manifold consists of three parts, namely, inlets, outlets, and connecting parts. The manifold's length and thickness are 95 cm and 0.6 cm, respectively. The simulation process was conducted in ANSYS 14, Fig. 3. All the steps, including creating geometry, mesh generation, and flow and solid analyses were carried out in this software. To start the simulation, first the geometry was drawn based on the available information of the manifold. In this step, all efforts were put to create the geometry with a high geometric similarity with the real manifold. Second, the created geometry was meshed using an unstructured mesh. Third, the meshed body was transferred to FLUENT and the flow and solid thermal analyses were done. Then, after meshing the solid body in ANSYS workbench, the flow and solid temperatures of the manifold were imported to the thermal and the structural sub-softwares of ANSYS workbench and after that the manifold thermal stresses and deformations were calculated under different operating conditions. Finally, the predicted critical sections were modified with attaching fins on them and then the above mentioned process was repeated once more to check out the solid thermal performance.

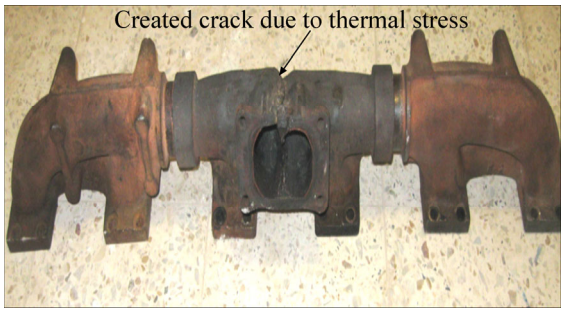

Fig. 1 Created crack due to thermal stresses in real manifold

3 Governing equations

In the reality, due to opening and closing the engine valves during an engine cycle (firing cycle), the manifold is working in an unsteady state. However, the unsteady simulation has high computational complexity and is not cost effective. In this work, a steady case was

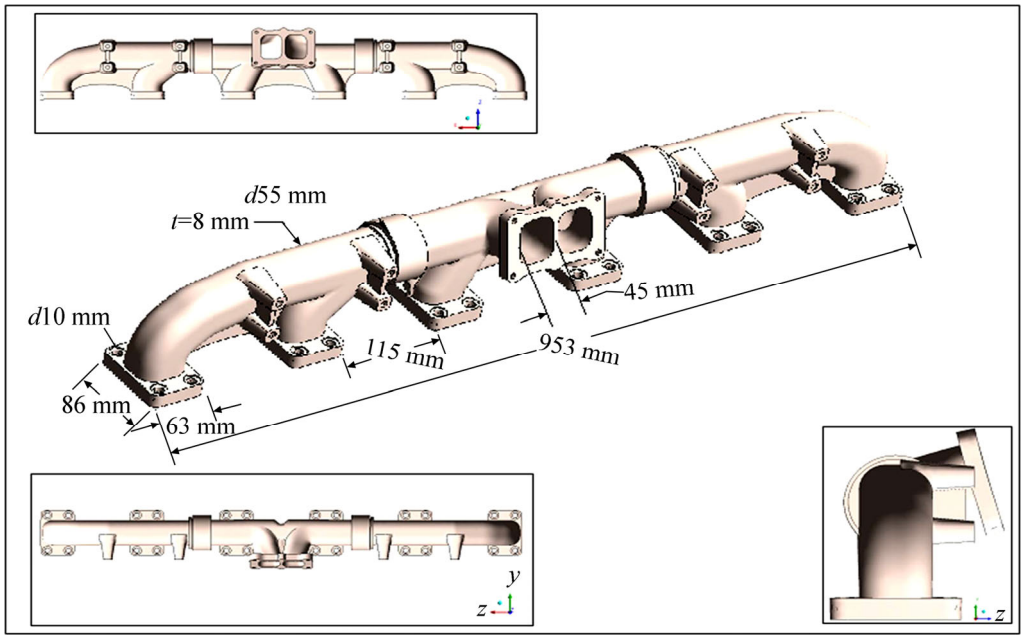

Fig. 2 Modeled geometry of exhaust manifold

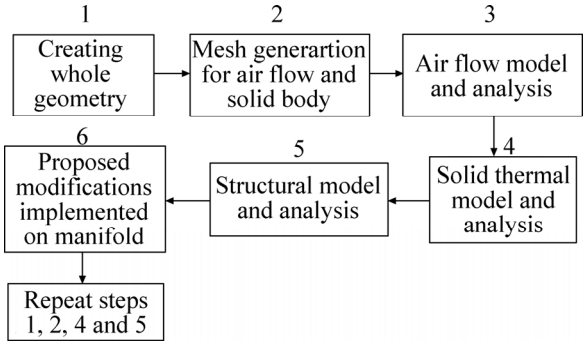

Fig. 3 Simulation process in ANSYS software

considered as an adequate situation to evaluate the manifold design [12]. The airflow and solid body modeling procedures are given in following.

3.1 Air flow

The following assumptions were made to solve the governing equations: the flow is turbulent, steady state, incompressible, and three-dimensional. The gravity acts in the vertical direction. The k–ε model was used to model the turbulent flow. The k–ε model is relatively simple to implement and leads to stable calculations that converge easily. The governing equations of the turbulent air flow inside the manifold are as follows:

$$\frac{\partial \bar{u}_i}{\partial x_i}=0 \tag{1}$$

$$\rho \bar{u}_j \frac{\partial \bar{u}_i}{\partial x_j}=\frac{\partial}{\partial x_j}\left[\mu_{\mathrm{t}}+\mu\frac{\partial \bar{u}_i}{\partial x_j}\right]-\frac{\partial p}{\partial x_i}+g_i\beta(T_{\mathrm{F}}-T_{\mathrm{o}}) \tag{2}$$

$$\rho \bar{u}_j \frac{\partial \bar{T}_{\mathrm{F}}}{\partial x_j}=\frac{\partial}{\partial x_j}\left[k_0+\mu_{\mathrm{t}}/\sigma_{\mathrm{T}}\frac{\partial T_{\mathrm{F}}}{\partial x_j}\right] \tag{3}$$

$$\rho \bar{u}_j \frac{\partial k}{\partial x_j}=\frac{\partial}{\partial x_j}\left[\mu_{\mathrm{t}}/\sigma_{k,\mathrm{t}}+\mu\frac{\partial k}{\partial x_j}\right]+G_k-\rho\varepsilon \tag{4}$$

$$\rho \bar{u}_j \frac{\partial \varepsilon}{\partial x_j}=\frac{\partial}{\partial x_j}\left[\mu_{\mathrm{t}}/\sigma_{k,\mathrm{t}}+\mu\frac{\partial \varepsilon}{\partial x_j}\right]+(C_1G_k\varepsilon-C_2\rho\varepsilon^2)/k \tag{5}$$

$$\mu_{\mathrm{t}}=\rho C_\mu\frac{k^2}{\varepsilon},\ C_2=1.9,\ C_1=1.4,\ \sigma_{k,\mathrm{t}}=1,\ \sigma_{\varepsilon,\mathrm{t}}=1.3,\ C_\mu=0.09$$

where u is velocity in x direction; ρ is fluid density; μ is fluid viscosity; μ_{t} is turbulent viscosity; p is pressure; g is gravitational acceleration; T_{F} is fluid temperature; T_0 is ambient temperature; k_0 is fluid conductivity; k is turbulent kinetic energy; ε is turbulent dissipation and the bar(−) denotes the Reynolds averaged property.

3.2 Manifold body

The following equations were used to analyze the shell of the manifold. Here, it was also assumed that the steady state condition is still held.

$$\frac{\partial}{\partial x_j}\left[k_{\mathrm{s}}\frac{\partial T_{\mathrm{s}}}{\partial x_j}\right]=0 \tag{6}$$

$$\frac{\partial}{\partial x_j}[\sigma_{ij}]+F_i=0 \tag{7}$$

$$\sigma_{ij}=\lambda e_{kk}\delta_{ij}+2\mu e_{ij}-(3\lambda+2\mu_{\mathrm{s}})\alpha(T_{\mathrm{s}}-T_0)\delta_{ij} \tag{8}$$

$$e_{ij}=\frac{1}{2}\left(\frac{\partial}{\partial x_j}[X_i]+\frac{\partial}{\partial x_i}[X_j]\right) \quad (9)$$

where k_s is sold conductivity, T_s is solid temperature, $\boldsymbol{\sigma}$ is stress tensor, $\boldsymbol{F}$ is the body forces, $\boldsymbol{e}$ is strain tensor, $\boldsymbol{X}$ is displacement, and $\boldsymbol{\delta}$ is the Kronecker delta.

It should be mentioned that Eq. (6) is solved independently from Eqs. (7), (8) and (9). Once the solid temperature is determined, the elastic analysis is done.

4 Material properties

The gas flow passed the exhaust manifold comes from the combustion chamber of the diesel engine. The complete combustion process was assumed. The adiabatic flame temperature of diesel fuel was taken as 2410 K. The stoichiometric ratio of the fuel to air was taken as 0.0669 for the diesel fuel. The fluid properties of the combustion products are given in Table 1.

Table 1 Properties of combustion product [13]

ρ/(kg·m^{-3})	μ/(Pa·s)	c_p/(J·kg^{-1}·K^{-1})	k/(W·m^{-1}·K^{-1})
1.0685	3.0927×10^{-5}	1056.6434	0.025

The manifold solid material is Si-Mo cast iron. The detailed composition of the manifold material is given in Table 2. The physical properties of the manifold are highly temperature dependent, Table 3. This fact is very important at high temperature cases. For instance, the manifold's elastic modulus highly decreases at temperatures above 750 °C as it is the case of this work. It should be pointed out that the temperature dependent properties of the solid were given to the numerical model by a separate file which helps the software to take into account the effect of temperature on the manifold properties properly. For doing this, the data given in Table 3 were given to the software. It also should be mentioned, it was assumed that the cast iron used in this study is the elastic-perfectly plastic.

5 Boundary conditions

Three types of loads are imposed on the manifold:

1) Mechanical stresses which are originated by the thermal stresses. The manifold highly suffers from relatively high operating temperatures, which creates significant thermal expansion and as the manifold is constrained, the expansion causes remarkable mechanical stress.

2) Mechanical stresses induced by the vibration of the exhaust system. It has been concluded that these kind of stresses induced by the vibration are of minor importance in the fatigue life of the exhaust manifold when the exhaust manifold is working under high operating temperatures [15].

3) Mechanical stresses due to air flow pressure. The pressure of the exhaust gas flow in the manifold varies between 100 kPa and 200 kPa. However, these pressure stresses are relatively low compared to the thermal stresses induced by the high operating temperatures.

4) Therefore, based on the above justifications, this study only considered the effects of thermal stress on the manifold fatigue life. Figure 4 shows the inlet and outlet sections of the manifold. The inlet temperature and total mass flow rate of combustion products at the maximum engine speed were taken as 750 °C and 0.053 kg/s, respectively, and in this case the flow regime is turbulent, i.e., Re=46129. All these data were borrowed from the engine manual. The turbulent intensities at the inlets were obtained 4% using the following equation [16]:

$$I=0.16(Re)^{-1/8} \quad (10)$$

It should be mentioned that the mass flow rate comes from the combustion chamber was equally divided into the six inlets and it was assumed that all the inlets received simultaneously one sixth of the total mass flow rate. The outflow boundary condition was selected

Table 2 Chemical composition of SiMo51 cast iron (mass fraction, %) [14]

Material	Structure	C	Si	Mn	Cr	Ni	Mo	Fe
SiMo51	Ferritic	3.43	2.1	0.68	0.33	0.05	0.36	Bal.

Table 3 Effect of temperature on manifold properties [14]

Temperature/ °C	Mass density/(kg·m^{-3})	Conductivity/ (W·m^{-1}·K^{-1})	Specific heat/ (J·kg^{-1}·K^{-1})	Elastic modulus/GPa	Poisson ratio	Thermal expansion/°C^{-1}	Yield stress/MPa
20	7100	48.5	460	160	0.3	12×10^{-6}	470
200	7100	48.5	460	145	0.3	12×10^{-6}	405
400	7100	48.0	510	140	0.3	12.7×10^{-6}	340
600	7100	47.7	536	125	0.3	13.5×10^{-6}	243
800	7100	47.7	536	35	0.3	14.2×10^{-6}	40

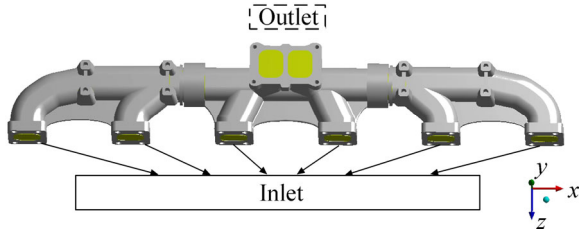

Fig. 4 Manifold inlet and outlet sections

in the manifold outlets.

The boundary conditions of solid body were divided in two parts, the structural and thermal boundary conditions. In the structural analysis, the inside and outside boundary conditions of the manifold body shell were given to the software. The inside boundary condition is the flow temperature adjacent to the wall, which is unknown till the fluid flow equations are solved. The outside boundary conditions are based on the heat transfer given to the surroundings by convection and radiation heat transfers. They are as follows:

$$k_s \frac{\partial T_s}{\partial n} = h_s(T_s - T_\infty) + \varepsilon\sigma(T_s^4 - T_\infty^4) \quad (11)$$

were h is convection heat transfer coefficient, ε is surface emissivity, A is area, σ is the Stephan Boltzmann constant, T_∞ is ambient temperature around the manifold, and T_s is solid temperature. The fixed boundary condition was used in the both inlet and outlet sections in the structural analysis. As stated before, the pressure force exerted on the inner surface of the exhaust pipes wall was ignored.

6 Numerical method

As mentioned earlier, the governing equations have been solved using ANSYS FLUENT 14. The governing equations of flow were discretized and converted into algebraic equations using the finite volume method. The unstructured grid type was used to generate the grids inside the manifold. The coupled velocity and pressure equations were solved using the SIMPLE algorithm. The generated grid for the air flow inside the manifold is shown in Fig. 5. Based on the geometry shape, an unstructured mesh was used. Finer meshes near the walls were implemented to resolve the effect of boundary layer.

The finite element analysis was carried out to calculate manifold thermal stress induced by exhausted gas using ANSYS workbench 14. The generated mesh for the manifold body shell is shown in Fig. 6. As shown in this figure, a high contracted mesh was selected in the likely high stress locations to resolve the stress and

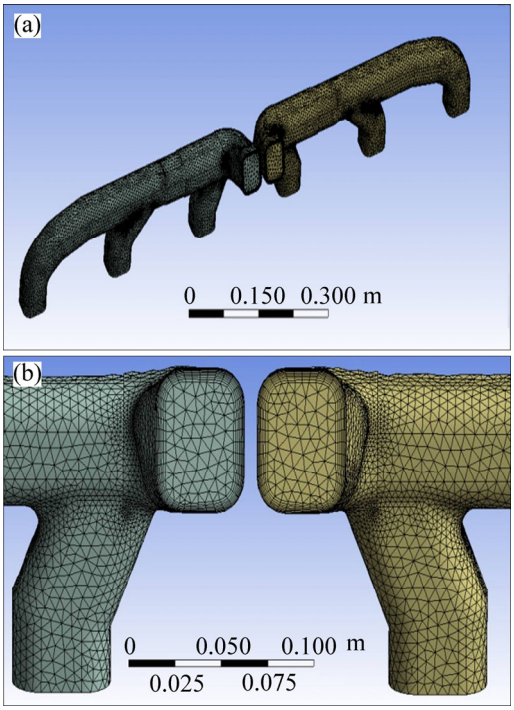

Fig. 5 Computational grid for air flow

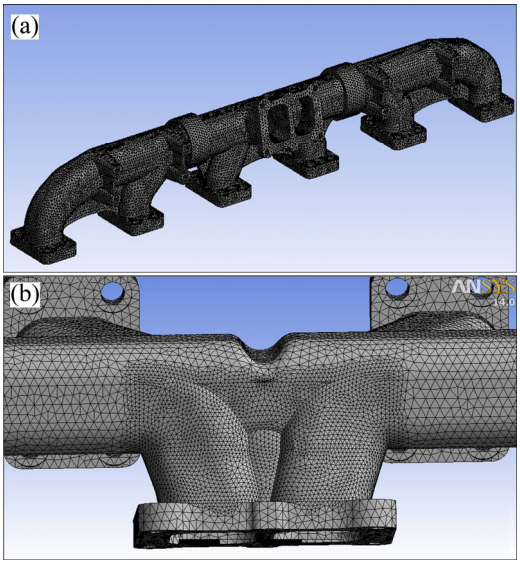

Fig. 6 Computational grid of body shell

deformation better.

The governing equations of flow were solved simultaneously and the computation was kept up till the residual of each corresponding properties approached 10^{-5}. The process mentioned above was repeated several times for different mesh sizes. To find the optimum mesh size, temperature of line AB in the manifold outlet section shown in Fig. 7(a), was obtained for different mesh sizes. Figure 7(b) shows the gas temperature distributions for different mesh sizes. As shown in this figure, the mesh size lower than 4mm gives a reasonable accuracy. However, the computation time should also be

incorporated in the calculation to find the optimum mesh size. Table 4 shows the computation times for different mesh sizes. As given in this table, the optimum mesh size is 4 mm with relatively low computation time and high accuracy. Figure 8 shows the calculation results of selecting the optimum mesh size of the manifold solid body. This was carried out after solving fluid flow inside the manifold and importing the corresponding outputs into the solid models. This figure states that the best mesh size is lower than 3 mm.

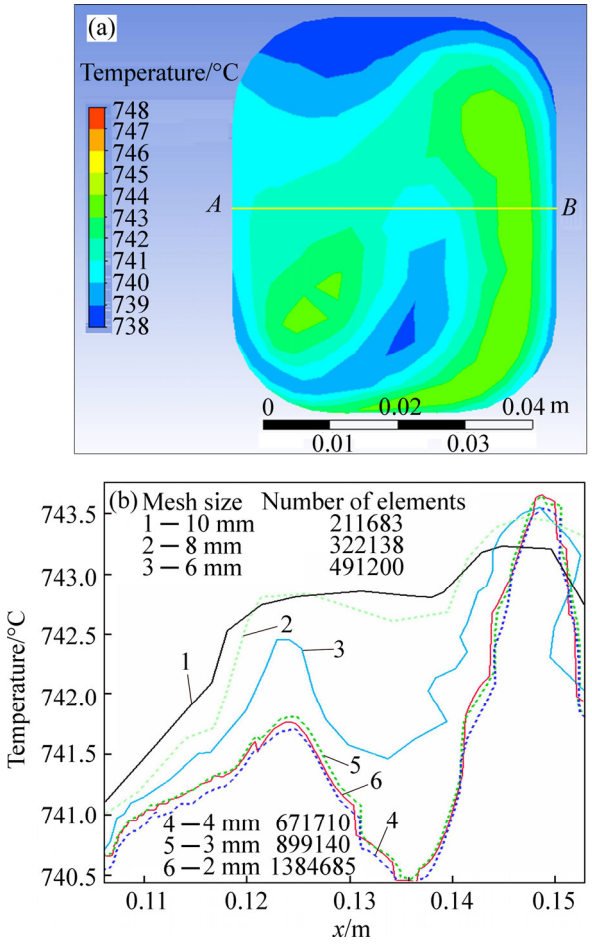

Fig. 7 Temperature distribution contour of outlet section (a) and temperature distribution along line *A*-*B* based on different mesh sizes (b)

Table 4 Computation times for different mesh sizes

Mesh size/mm	Temperature/°C	Friction coefficient, C_F	Computation time/h	Number of cells
2	741.3	0.048	22.25	1384685
3	741.7	0.049	18	899140
4	740.8	0.051	9.5	671710
6	742.1	0.059	7.5	491200
8	742.3	0.066	6.2	322138
10	742.8	0.068	4	211683

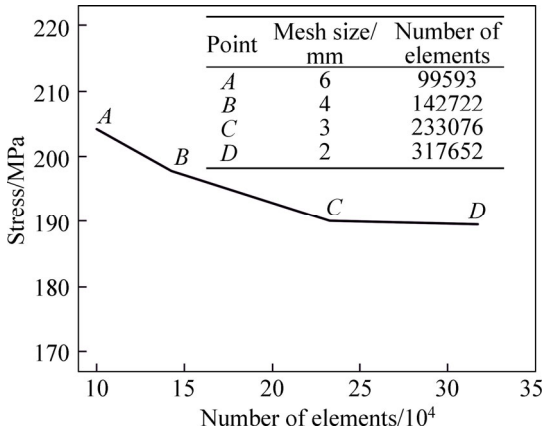

Fig. 8 Maximum thermal stress of manifold based on different mesh sizes

7 Results and discussion

In this section, the numerical results of airflow inside the manifold are analyzed. The air velocity distribution is shown in Fig. 9. As shown in this figure, the velocity increases as the flow pushes forward through the manifold tubes and approach to the maximum speed at the outlet sections. Pressure distribution of air flow at section A is shown in Fig. 10. As shown in this figure, the pressure gets a negative value in the outlet sections as it was supposed before. This makes the outlet section more susceptible against mechanical stresses. However, it seems that it is ignorance compared to the thermal stresses. The temperature of the combustion products through the interior of the manifold is shown in Fig. 11. As shown in this figure, the temperature is approximately uniform and is in the range of 749 to 750 °C all over the manifold interior.

7.1 Solid analysis for finding critical spots

In this section, the thermal stresses of the manifold body are investigated. For doing this, the inner wall temperature of the manifold which was calculated in air flow modeling section was imported to the solid model as an inside boundary condition. The outer surfaces of manifold are subjected to the convection and radiation heat transfers. After solving the solid governing equations, the solid temperature, the thermal stress, and thermal deformation were obtained. The temperature distribution of manifold is shown in Fig. 12. As shown in this figure, the maximum temperature is seen in the outlet section. The thermal stresses and thermal deformations are shown in Figs. 13 and 14, respectively. As shown in these figures, the maximum thermal stress and the maximum thermal deformation happen in the outlet section. The created crack on the real manifold was also seen in this section and this qualitatively confirms that the simulation was conducted properly. As

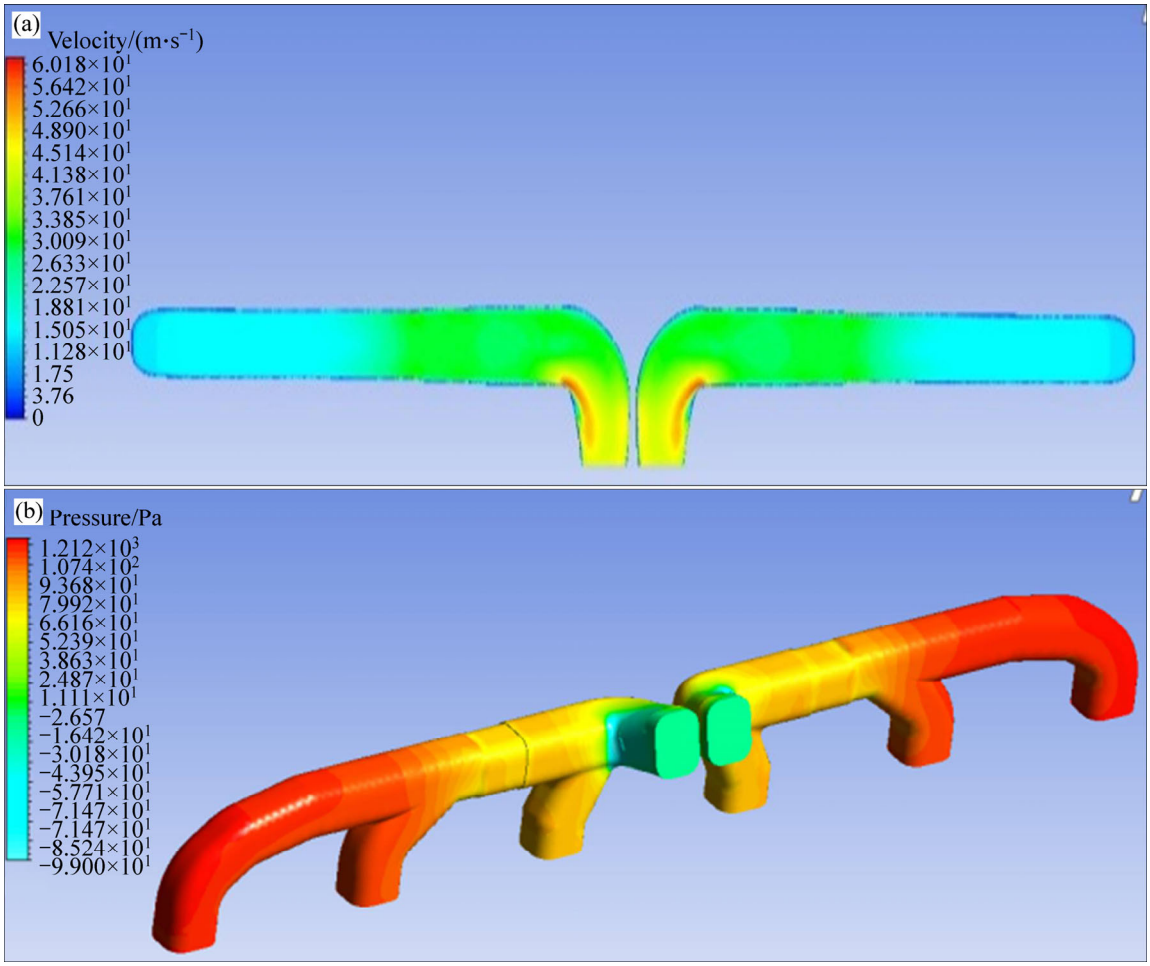

Fig 9 Velocity (a) and pressure (b) distributions of airflow inside manifold

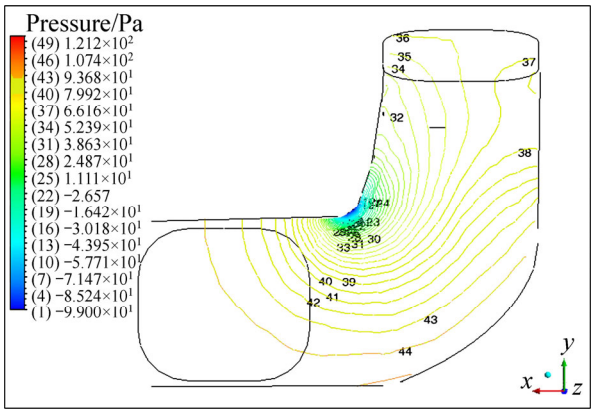

Fig. 10 Pressure distribution in outlet section (Section A)

mentioned before, the convection heat transfer coefficient and the ambient temperature have a great impact on the manifold thermal stress. As shown in Fig. 15, higher ambient temperatures surrounding the engine increases the manifold thermal stress by up to 10%. Also increasing the convection heat transfer decreases the thermal stresses by up to 8%. The maximum deformation of the manifold body at different fluid temperatures is shown in Fig. 16. As shown in this figure, increasing the temperature enhances the thermal deformation. This is intensified at temperatures higher than 750 °C due to a significant decrease of the manifold elastic modulus (Table 3). The safety factor was also obtained and shown in Fig. 17. As shown in this figure, the outlet section has the minimum safety factor as it experiences the maximum thermal stress.

7.2 Verification of simulation results

In order to verify the simulation results and check the predicted crack occurred in the original manifold, some thermal images were taken from the exhaust manifold while the engine was working at a moderate speed, using a high resolution thermovision camera. The obtained results were compared with the simulation results. Figure 18 therefore shows a qualitative comparison between the damaged manifold, the simulated manifold, and the thermovosion images. As shown in this figure, there is a good compromise between the simulation and the real situation. It is clear from the both images that the high stress area is on the shell of outlet section and this means that the simulation results are trustworthy.

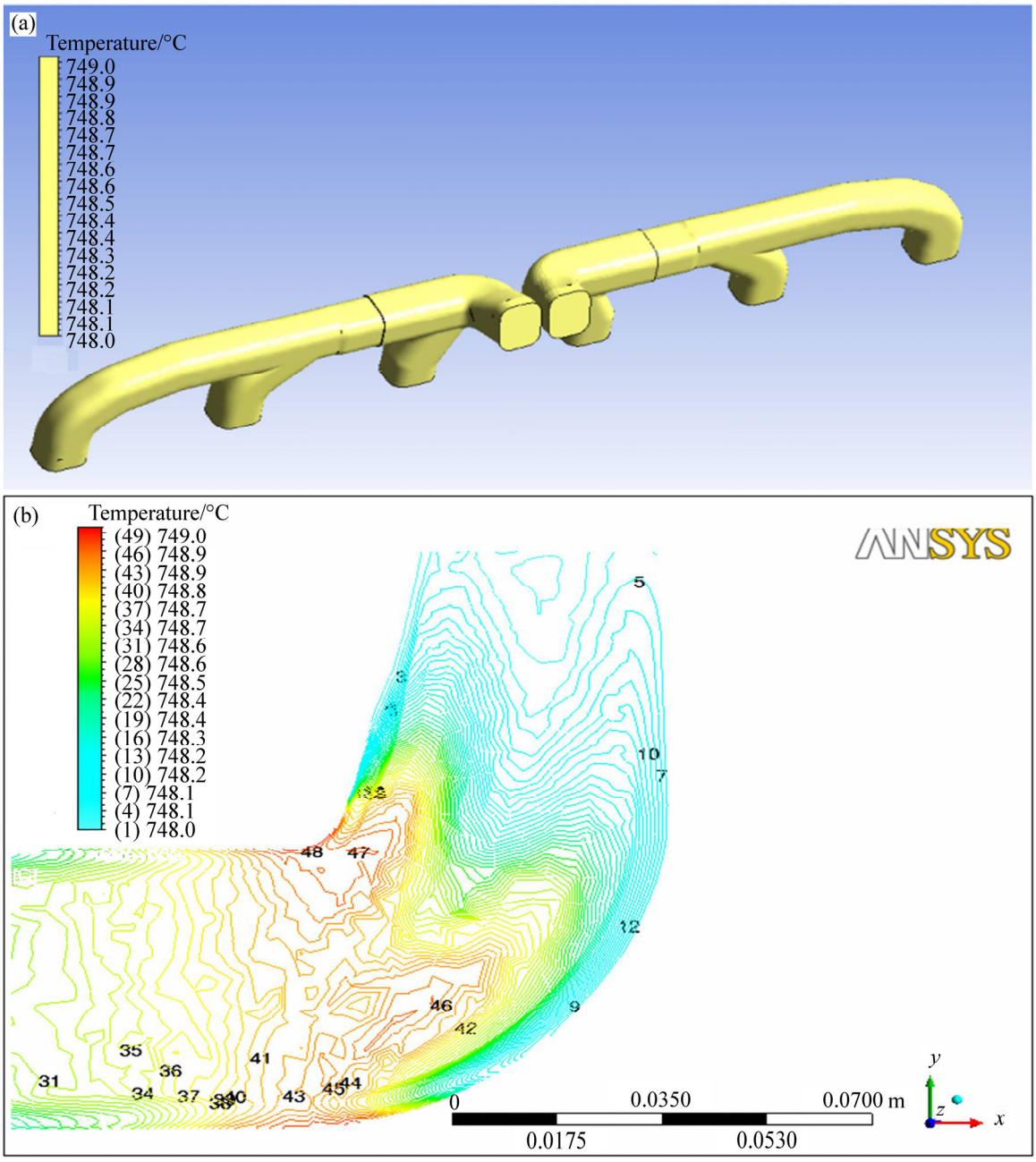

Fig. 11 Temperature distribution of airflow: (a) Inside whole manifold; (b) Section A

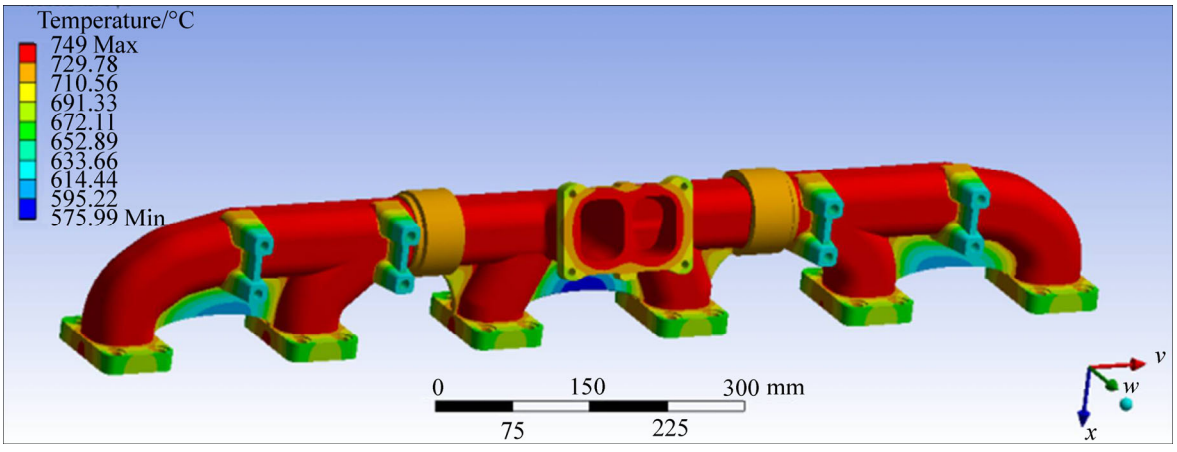

Fig. 12 Solid temperature distribution

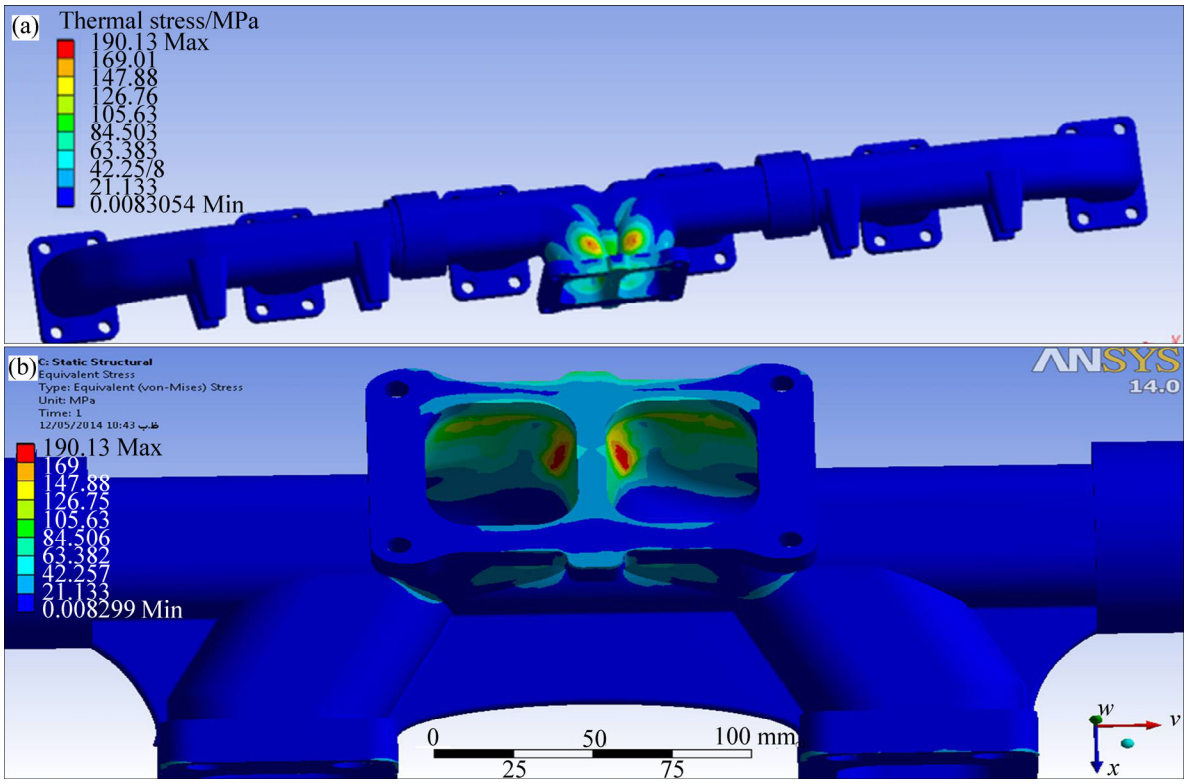

Fig. 13 Thermal stress distribution of manifold

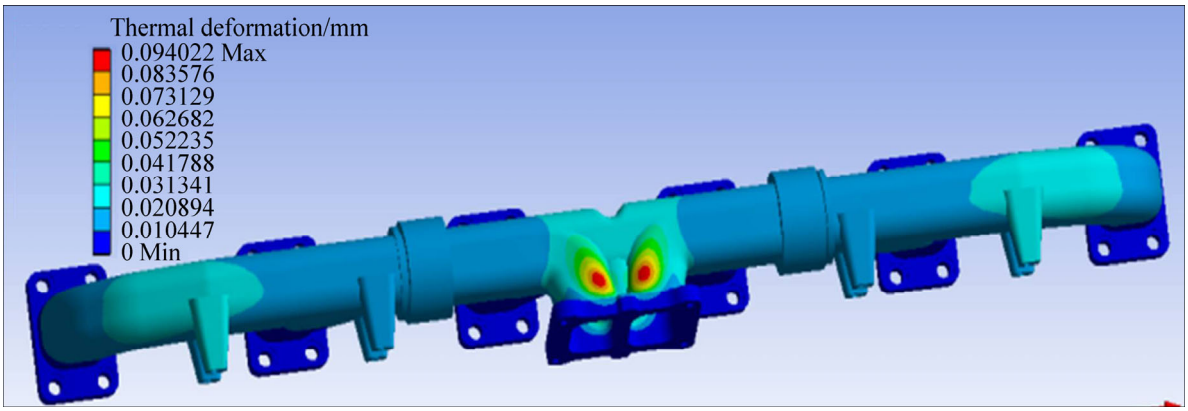

Fig. 14 Thermal deformation distribution of manifold

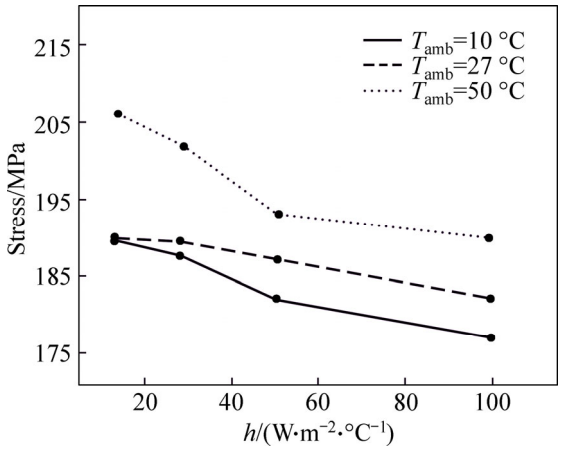

Fig. 15 Maximum thermal stress versus convection heat transfer coefficient at different ambient temperatures

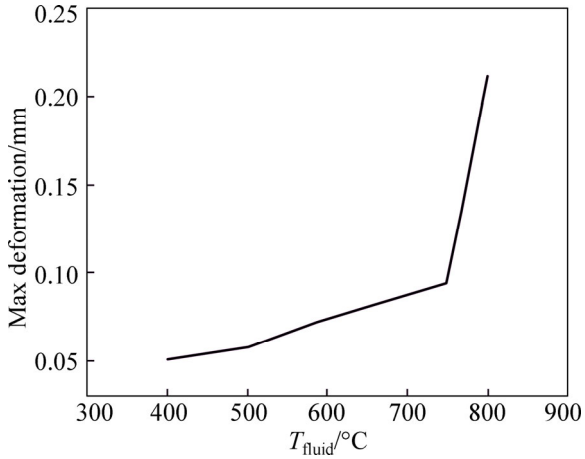

Fig. 16 Maximum thermal deformation versus fluid flow temperature

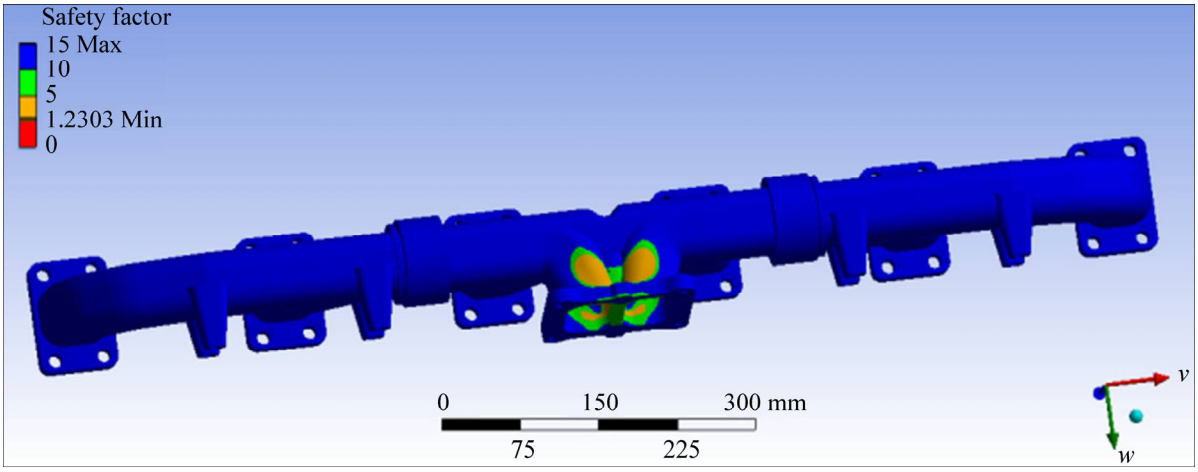

Fig. 17 Safety factor distribution of manifold

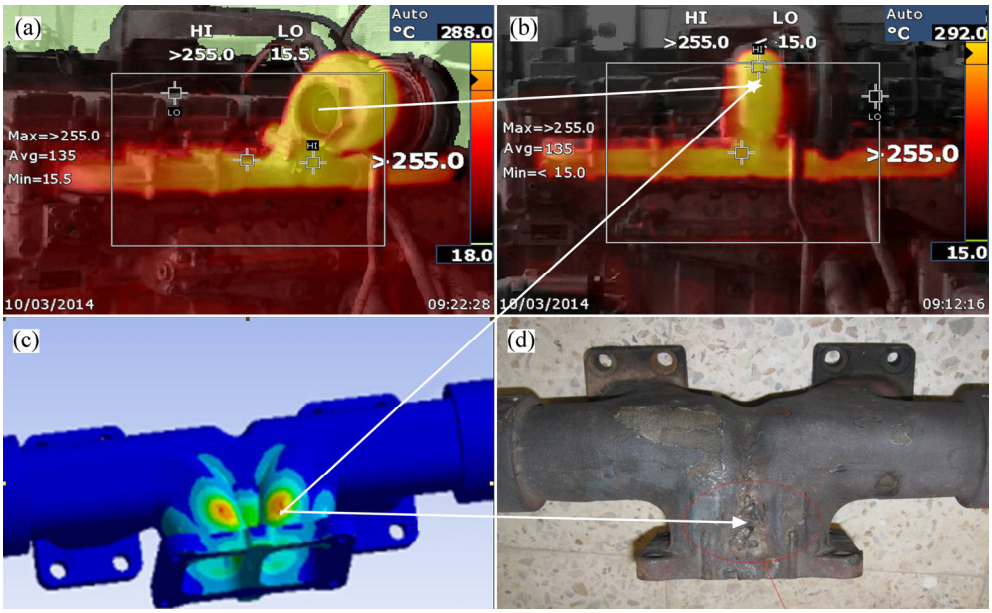

Fig. 18 Verification of simulation results qualitatively by comparing them with created cracks in damaged real manifold and its thermovision images

7.3 Fin attachment to critical areas

As shown earlier in Fig. 18, the thermal stresses created a crack in the middle of the gas outlet section shell. This crack needs to be treated otherwise the manifold would be damaged severely. To reduce the induced thermal stresses on the outlet section, some modifications were incorporated into the manifold's outlet section. Two modifications were implemented. First, the thickness of the manifold outlet wall was increased uniformly and then two different fins (i.e. Perimeter fins and curved fins) were attached to the outlet section as shown in Fig. 19. The increased thickness solely could not harness the thermal stresses as there is a limitation for increasing the wall thickness. Thus, three circular fins with 5 mm thickness were attached to the manifold outlet section. The temperature distributions of these modifications are shown in Fig. 20.

To show the effect of fin attachment and thickness increase clearer on the manifold stress, the outlet section was cut across its axial surface (Fig. 21) and the temperature, thermal stress, thermal deformation, and safety factors were plotted across the line *AB* in Figs. 22, 23, and 24, respectively. The temperature distributions of three cases, namely the original manifold, the manifold with increased thickness, and the manifold with fins attachments as well as thickness increase are shown in Fig. 21. As shown in this figure, the manifold with increased wall thickness reduces the induced temperature about 3 °C while the manifold with fin attachment and increased wall thickness has about 32 °C lower temperature compared to the no finned manifold. The thermal stress and thermal deformation distributions for the perimeter fins are shown in Figs. 19 and 20, respectively. As shown in these figures, the thermal

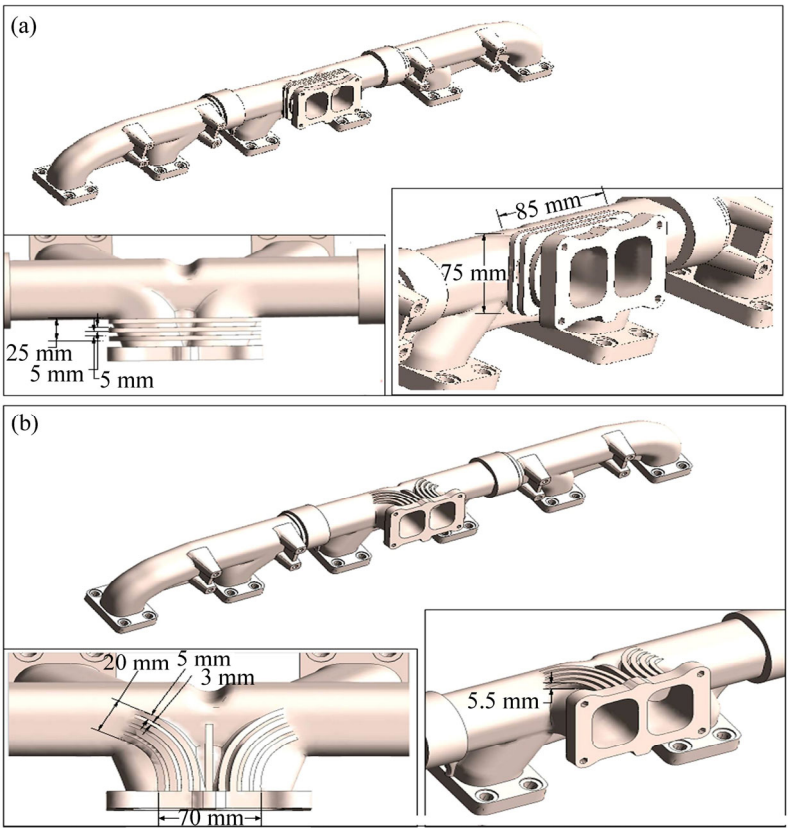

Fig. 19 Modified manifolds with perimeter fin attachment (a) and curved fin attachment (b)

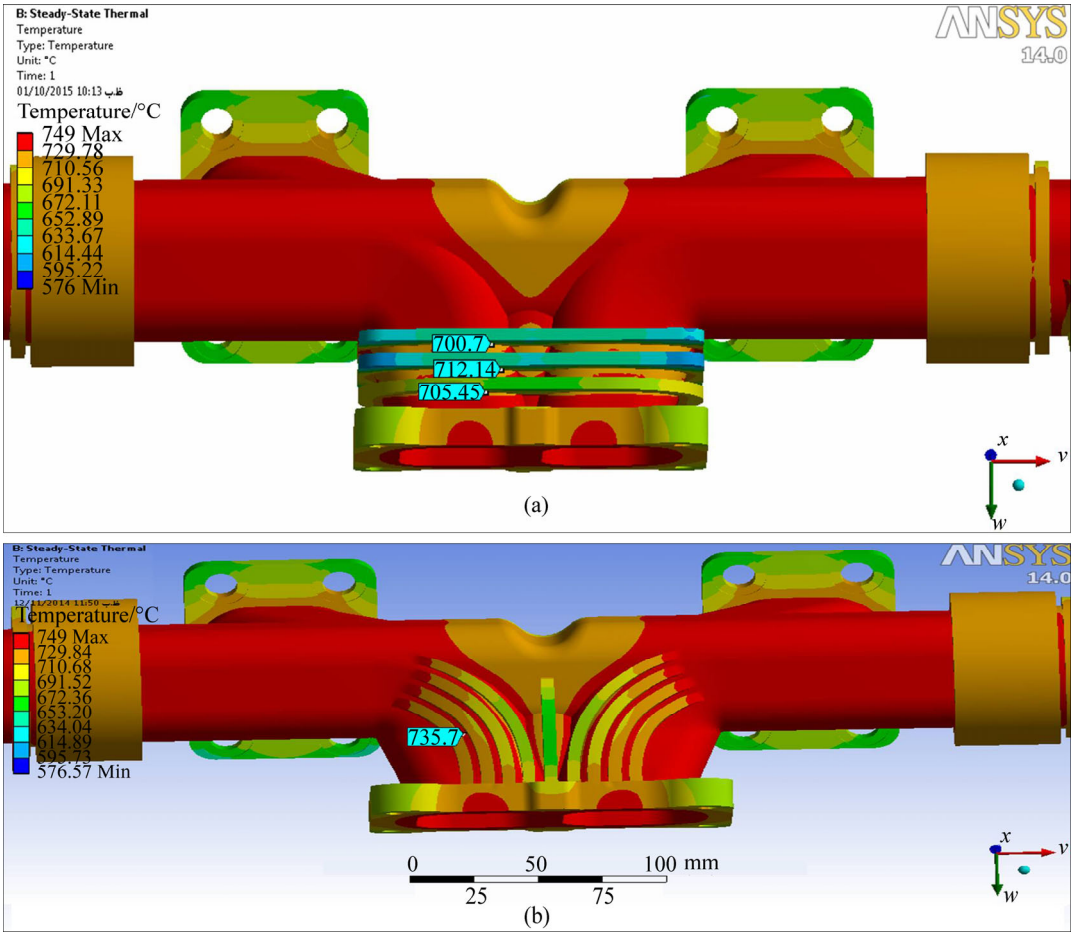

Fig. 20 Temperature distributions of manifold with two fin attachments: (a) Perimeter fin; (b) Curved fin

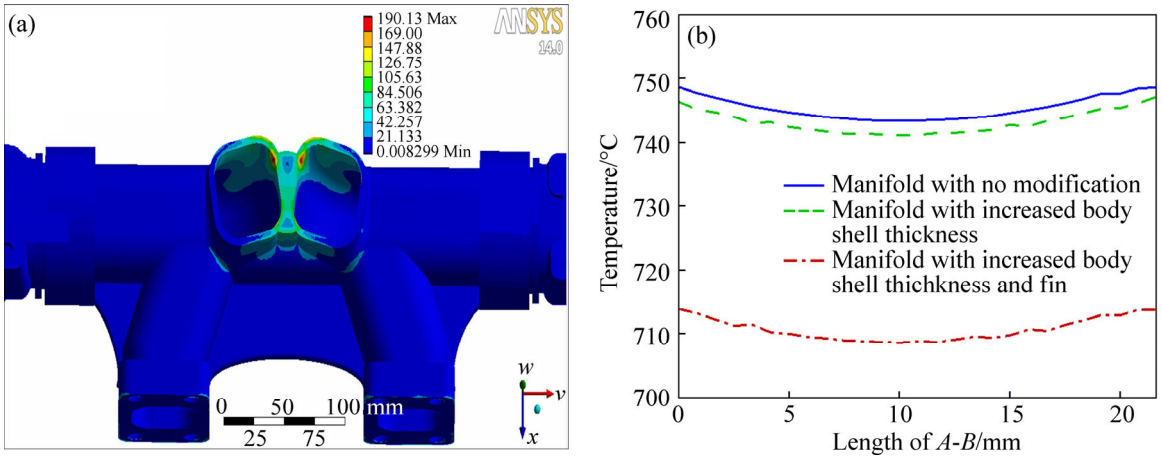

Fig. 21 Temperature distributions: (a) Whole manifold with fine attachment; (b) Along line *A*-*B* for manifold with no modifications, manifold with body shell thickness increase, and manifold with increased body shell thickness and fin attachment

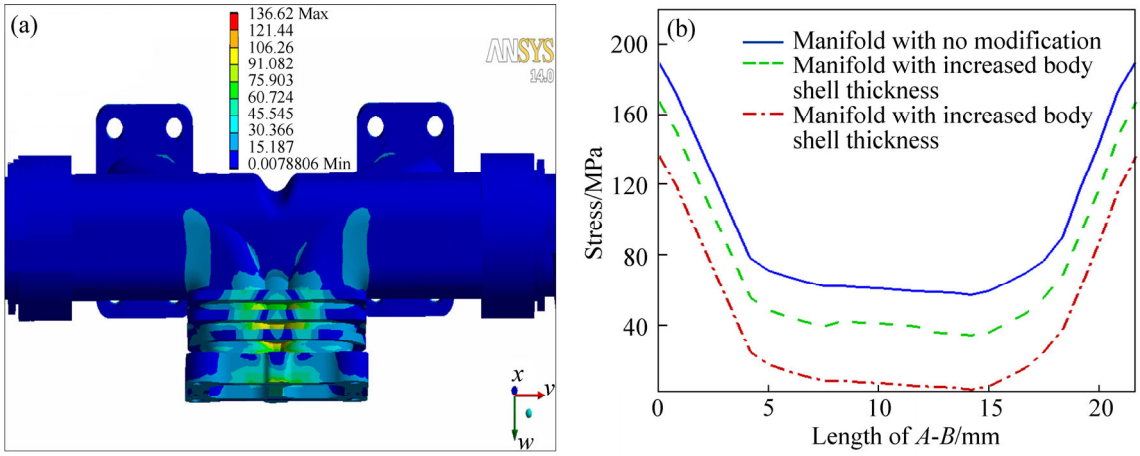

Fig. 22 Thermal stress distribution: (a) Whole manifold with fin attachment; (b) Along line *A*-*B* for manifold with no modifications, manifold with body shell thickness increase, and manifold with increased body shell thickness and fin

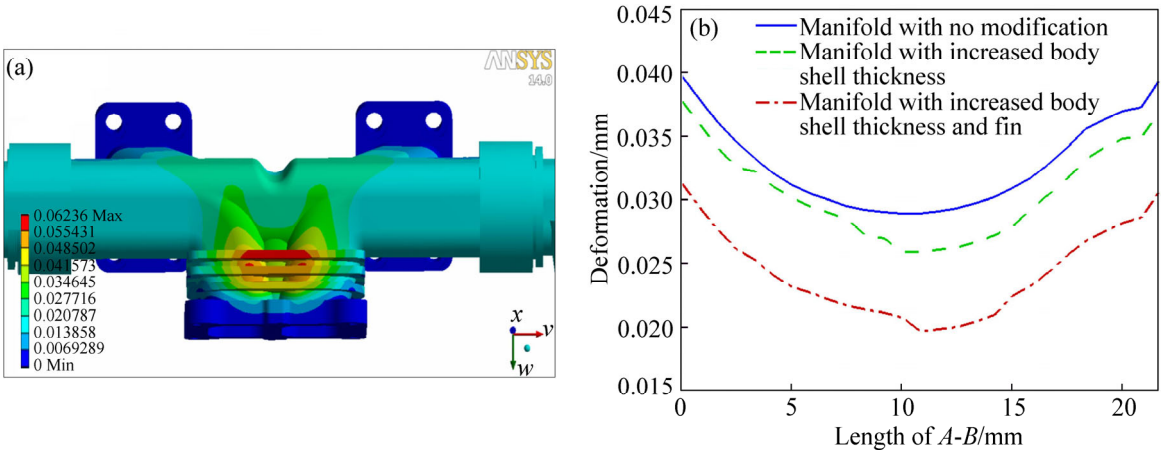

Fig. 23 Thermal deformation distribution: (a) Whole manifold with fin attachment; (b) Along line *A*-*B* for manifold with no modifications, manifold with body shell thickness increase, and manifold with increased body shell thickness and fin attachment

stress and the corresponding thermal deformation in the outlet section have degraded as the results of the modifications. The safety factor distribution in this case is shown in Fig. 24. It is clearly seen that the minimum safety factor is highly increased and the manifold resists well against the thermal stresses all over its body. The comparison of thermal performances between the perimeter and curved fins was also carried out and given in Table 5. It is shown that the perimeter fins are much more effective than the curved fins in the reduction

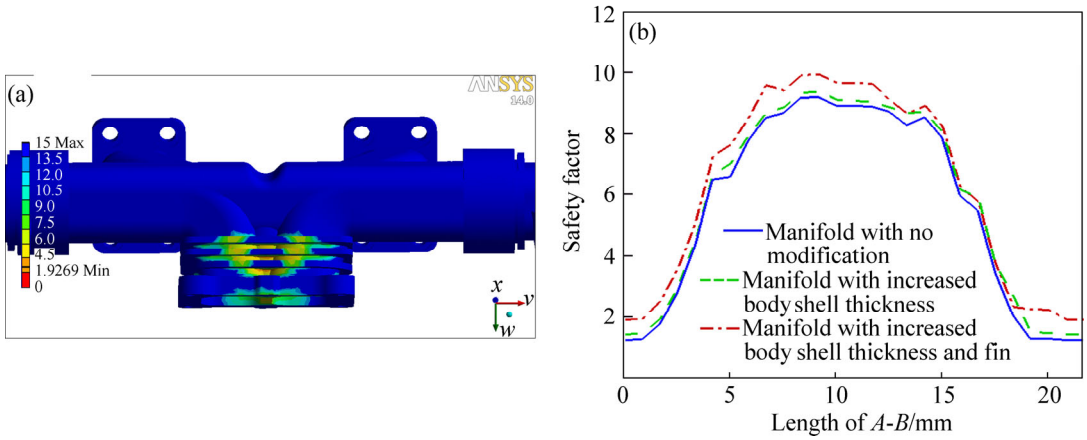

Fig. 24 Safety factor distributions: (a) Whole manifold with fin attachment; (b) Along line *A*-*B* for manifold with no modifications, manifold with body shell thickness increase, and manifold with increased body shell thickness and fin attachment

Table 5 Comparison of maximum thermal stress, safety factor, and weight of manifold with perimeter and curved fin attachments

Manifold	Stress/MPa	Safety factor	Weight/N
Original manifold	190.13	1.23	180.29
Manifold with perimeter fins	148.75	1.62	184.43
Manifold with curved fins	180.46	1.38	182.15
Manifold with increased shell thickness	167.56	1.44	191.56
Manifold with circular fins and increased shell thickness	136.62	1.92	195.7
Manifold with curved fins and increased shell thickness	161.83	1.52	193.42

of the thermal stresses. The thermal stresses of the manifold with the perimeter fins are 22% lower than the manifold with curved fins. This table also states that the fin attachment does not increase the manifold's weight significantly.

8 Conclusions

1) The outlet section of the manifold has the maximum temperature and correspondingly the maximum thermal stress and deformation.

2) The predicted area of critical stress was also confirmed with the crack seen area of the real manifold.

3) The manifold was modified in the simulation process to harness the high thermal stress and the high thermal deformation. Two types of fines as well as increasing the solid body thickness were applied in the critical areas. To evaluate these modifications, the manifold shell thickness was increased and then some fins were attached to the outlet section of the manifold.

4) It was concluded that the fin attachment decreases the thermal stresses by 17% and further reduction depends on the type of fin used.

5) The results also indicated that the combined modifications, i.e. the thickness increase and the fins attachments, decrease the thermal stresses by up to 28% and the contribution of the fin attachment in this reduction was much higher compared to the shell thickness increase.

References

[1] KANDYLAS I P, STAMATELOS A M. Engine exhaust system design based on heat transfer computation [J]. Energy Conversion & Management, 1999, 40: 1057−1072.

[2] LONDHE A. Thermo-structural strength analysis for failure prediction and concern resolution of an exhaust manifold [R]. Automotive Sector Nasik, India, 2003: 3580−3588.

[3] YASAR D, BURKHARD S, JIMENEZ L P. CFD-FE-analysis for the exhaust manifold of a diesel engine [J]. International Journal of Mechanical Sciences, 2004, 47: 303−317.

[4] ZHANG X. Coupled thermo-fluid-solid analysis of engine exhaust manifold considering welding residual stresses [J]. Transactions of JWRI, Special Issue on WSE, 2011: 75−77.

[5] MAOQINA Z. Development for stainless steel exhaust manifold and CAE analysis [J]. Advance Material Research, 2012, 164(4): 123−128.

[6] RATHNARA J D. Thermomechanical fatigue analysis of stainless steel exhaust manifolds [J]. IRACST–Engineering Science and Technology, An International Journal (ESTIJ), 2012, 2(2): 265−267

[7] SATISH S. Comparison of predictions obtained on an exhaust manifold analysis [C]// International Congress on Computational Mechanics and Simulation (ICCMS). IIT Hyderabad, 2012.

[8] LIU Z E. Numerical simulation for exhaust manifold based on the serial coupling of STAR-CCM+ and ABAQUS [J]. Research Journal of Applied Sciences, Engineering and Technology, 2013, 6(20): 3903−3912.

[9] JAIN S, AGRAWAL A. Coupled thermal–structural finite element

analysis for exhaust manifold of an off-road vehicle diesel engine [J]. International Journal of Soft Computing and Engineering (IJSCE), 2013, 3: 226−223.

[10] ZOU B. The impact of temperature effect on exhaust manifold thermal modal analysis [J]. Research Journal of Applied Sciences, Engineering and Technology, 2013, 6(15): 2824−2829.

[11] LUJÁN J M, CLIMENT H, OLMEDA P. Heat transfer modeling in exhaust systems of high-performance two-stroke engines [J]. Applied Thermal Engineering, 2014, 69(1, 2): 96−104.

[12] DONG F, HUANG D, JUMA A, SCHREIBER C M, WANG X L, ZHOU C Q. Numerical simulation of thermal stress for a liquid-cooled exhaust [C]// Proceedings of IMECE2008, 2008 ASME International Mechanical Engineering Congress and Exposition. Boston, Massachusetts, USA, 2008.

[13] UMESH K S. CFD analysis and experimental verification of effect of manifold geometry on volumetric efficiency and for multi-cylinder engine [J]. International Journal of Engineering & Science Research, 2013, 3: 342−353.

[14] BRANDES E A, BROOK G B. Smithells metal reference book [M]. Oxford, Butterworth Heinemann, 1992.

[15] WOLFF K, HUSER M. Computer aided development of exhaust system durability [M]. GPC, 1998.

[16] POPE S B. Turbulent flows [M]. Cambridge, UK, Cambridge University Press, 2000.

(Edited by YANG Bing)

Cite this article as: Ali Akbar Partoaa, Morteza Abdolzadeh, Masoud Rezaeizadeh. Effect of fin attachment on thermal stress reduction of exhaust manifold of an off road diesel engine [J]. Journal of Central South University, 2017, 24(2): 546−559. DOI: 10.1007/s11771-017-3457-1.